Energy dependence of the nucleus-nucleus potential close to the Coulomb barrier

Kouhei Washiyama[1,2,*] and Denis Lacroix[1]
[1]*GANIL, CEA and IN2P3, Boîte Postale 55027, F-14076 Caen Cedex 5, France*
[2]*Department of Physics, Tohoku University, Sendai 980-8578, Japan*
(Received 17 April 2008; revised manuscript received 4 July 2008; published 29 August 2008)

The nucleus-nucleus interaction potentials in heavy-ion fusion reactions are extracted from the microscopic time-dependent Hartree-Fock theory for the mass symmetric reactions $^{16}O + ^{16}O$, $^{40}Ca + ^{40}Ca$, and $^{48}Ca + ^{48}Ca$ and the mass asymmetric reactions $^{16}O + ^{40,48}Ca$, $^{40}Ca + ^{48}Ca$, $^{16}O + ^{208}Pb$, and $^{40}Ca + ^{90}Zr$. When the c.m. energy is much higher than the Coulomb barrier energy, potentials deduced with the microscopic theory identify with the frozen density approximation. As the c.m. energy decreases and approaches the Coulomb barrier, potentials become energy dependent. This dependence indicates dynamical reorganization of internal degrees of freedom and leads to a reduction of the "apparent" barrier felt by the two nuclei during fusion of the order of 2–3% compared to the frozen density case. Several examples illustrate that the potential landscape changes rapidly when the c.m. energy is in the vicinity of the Coulomb barrier energy. The energy dependence is expected to have a significant role on fusion around the Coulomb barrier.

DOI: 10.1103/PhysRevC.78.024610 PACS number(s): 25.70.Jj, 21.60.Jz

I. INTRODUCTION

Heavy-ion fusion reactions give important information on dynamical evolution and dissipative phenomena in a quantum many-body system. Macroscopic models [1–5] using suitable estimates of nucleus-nucleus potentials [3,6–12] and then coupled-channels theories [13–15] have been widely used to describe the entrance channel of fusion reactions. These models indicate that the interplay between nuclear structure and dynamical effects is crucial to properly describing fusion reactions at energies close to the Coulomb barrier. While in general rather successful, these methods have in common several drawbacks. First, nuclear structure and dynamical effects should be treated in a unified framework. Second, important effects should be guessed *a priori*. This has been illustrated recently to understand new high-precision measurements at extreme subbarrier energies [16–20], where different effects such as incompressibility [21], nucleon exchange [22], and the transition from dinuclear to compound nucleus descriptions [23] have been invoked to understand experimental observations [16–20]. Then, the hypothesis could only be checked *a posteriori*. From this point of view, it is first desirable to use theories that consider both nuclear structure and nuclear dynamics in a unified framework. Second, the use of theories that automatically incorporate all the physical effects mentioned above can be of particular interest for disentangling different contributions.

Mean-field theories based on the Skyrme energy density functional (EDF) provide a rather unique tool for describing nuclear structure and nuclear reactions over the whole nuclear chart. In nuclear reactions, application of the so-called time-dependent Hartree-Fock (TDHF) to heavy-ion fusion reactions more than 30 years ago [24–30] was a major step. As computer power has increased, a more accurate description of nuclear reactions has been achieved. Most recent TDHF simulations include the spin-orbit force [31–36] and break all the symmetries (plane and axis symmetries generally assumed to speed up calculations). Moreover, all the terms of the Skyrme EDF used in nuclear structure can now be included [37–44]. The ability to perform full three-dimensional calculations and to use effective forces consistent with nuclear structure is crucial to accounting for the richness of nuclear shapes that are accessed dynamically. In addition, the great interest in dynamical mean-field theories with respect to other methods is that many factors known to affect fusion such as dynamical deformation, nucleon exchange, and nuclear incompressibility are automatically incorporated.

The original purpose of the present work was to benchmark the method proposed in Refs. [29,33] to obtain nucleus-nucleus potential and one-body dissipation from the microscopic TDHF dynamics. The possibility of obtaining such a potential from a mean-field theory has been studied in several works using the static EDF technique [45–48]. More recently, a method called density-constrained TDHF (DC-TDHF) [49], which combines TDHF dynamics with a minimization technique under constraints on the one-body density, has been applied in Refs. [41,42]; the DC-TDHF method is able to incorporate possible dynamical effects through the use of realistic density profiles obtained during the evolution.

Here, we consider a different approach based on a macroscopic reduction of the mean-field dynamics, called hereafter dissipative-dynamics TDHF (DD-TDHF). This technique could *a priori* give access to not only the nucleus-nucleus potential but also the friction coefficients which play an important role in macroscopic models [50–53] and have rarely been obtained from fully microscopic theories [29,54]. The main difficulty of the macroscopic reduction is to guess the relevant collective degrees of freedom and their equation of motion. Most models assume that the fusion problem can be reduced to a one-dimensional problem on the relative distance between nuclei. Here, we will test this hypothesis in TDHF and suppose that the dynamics is described by a one-dimensional macroscopic dissipative dynamics. Since

*washiyama@ganil.fr

there is freedom in the choice of macroscopic equations, the simple assumption made should first be validated. Thanks to alternative techniques used to infer Coulomb barriers from TDHF [36,41], we show that the DD-TDHF method can be a useful tool for obtaining precise information on potentials felt during fusion. In particular, because of dynamical effects, the deduced nucleus-nucleus potentials depend explicitly on the c.m. energy close to the Coulomb barrier. This energy dependence, which was discussed in different models [55,56], is studied in detail.

In this article, we concentrate on the study of nuclear potentials. Aspects related to dissipation will be discussed in Ref. [57]. The paper is organized as follows. The next section introduces the DD-TDHF method. In Sec. III, we give the results and discuss the extracted quantities. A summary is given in Sec. IV.

II. NUCLEUS-NUCLEUS POTENTIAL FROM THE MICROSCOPIC MEAN-FIELD MODEL

In this section, the extraction of nucleus-nucleus interaction potentials from mean-field theories is discussed. In macroscopic models, these potentials are generally displayed as a function of a few macroscopic collective degrees of freedom describing, e.g., the relative distance, shapes of nuclei, and mass asymmetry. Here, we will concentrate on head-on collisions between initially spherical nuclei[1] and assume that the collective space simply identifies with the relative distance R between colliding nuclei. The validity of this approximation in the TDHF context will be discussed below. In the following, we first present a general discussion on different methods of extracting nucleus-nucleus potential from a mean-field theory.

A. Some remarks on EDF

The basic ingredient of a nuclear mean-field model is the energy functional of the one-body density $\hat{\rho}$ denoted by $\mathcal{E}[\hat{\rho}]$. In the nuclear context, $\mathcal{E}[\hat{\rho}]$ is expressed in terms of a few parameters generally related to the associated effective interaction. Here, we will use the Skyrme EDF with the SLy4d [31] parameters. This choice is particularly suited to dynamical calculations because of the removal of c.m. corrections in the fitting procedure of the force parameters [31]. In the EDF context, static properties of nuclei are deduced by minimizing the functional with respect to all possible one-body densities. The great interest of EDF theory is that the initial complicated many-body problem is replaced by an independent particle problem. Indeed, the minimization procedure is equivalent to finding the set of single-particle states that diagonalizes both the self-consistent mean-field defined through the relation $h[\hat{\rho}]_{ij} = \partial\mathcal{E}[\hat{\rho}]/\partial\rho_{ji}$ and the one-body density. At the minimum, we have $[\hat{h}[\hat{\rho}], \hat{\rho}] = 0$.

[1]Note that nuclei might be deformed during the reaction.

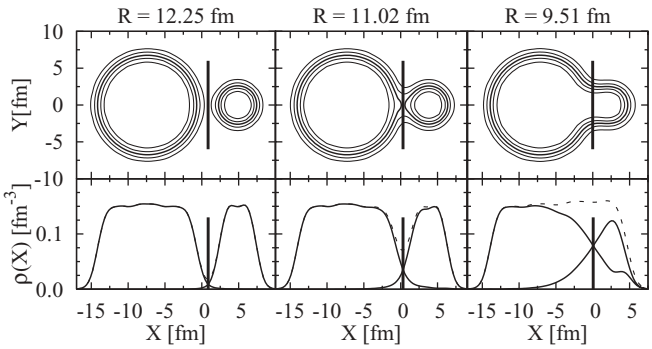

FIG. 1. Top: Density profiles $\rho(X, Y, 0)$ obtained with TDHF for the $^{16}O + ^{208}Pb$ head-on collision at $E_{c.m.} = 120$ MeV at three different relative distances. The isodensities (contour lines) are plotted at each 0.025 fm^{-3}. The vertical lines indicate the positions of separation planes (see text). Bottom: Total one-dimensional density $\rho(X, 0, 0)$ (dashed line) obtained at the same relative distances. In each case, the two solid curves denote, respectively, $\rho_T(X, 0, 0)$ and $\rho_P(X, 0, 0)$ (see text). Again, the separation plane is presented by the vertical line.

B. Illustration of fusion with time-dependent EDF

The static EDF theory has also its dynamical counterpart, called time-dependent EDF[2] where the dynamical evolution of nuclear systems is replaced by the one-body density evolution, i.e.,

$$i\hbar\frac{d\hat{\rho}}{dt} = [\hat{h}[\hat{\rho}], \hat{\rho}]. \quad (1)$$

Dynamical calculations presented in this paper are performed with the three-dimensional TDHF code developed by P. Bonche and coworkers with the SLy4d Skyrme effective force [31]. For the initial conditions for the TDHF time evolution, we prepare the density of colliding nuclei by solving static HF equations with the same effective force as the one used in the TDHF. The step size in the coordinate space is 0.8 fm. Then, we calculate the time evolution of the colliding nuclei in the three-dimensional mesh. The time step is 0.45 fm/c and the initial distance is set between 16 and 22.4 fm, depending on the reaction. We assume that the colliding nuclei follow the Rutherford trajectory before they reach the initial distance for TDHF. Thus, the initial positions and the momenta of the colliding nuclei are determined. As an illustration, the density evolution of the $^{16}O + ^{208}Pb$ head-on collision at c.m. energy $E_{c.m.} = 120$ MeV are shown at three different relative distances in Fig. 1.

C. Discussion of nucleus-nucleus potentials deduced from mean-field theories

A good estimate of the interaction potentials felt by the two nuclei in the approaching phase within the EDF theory could be obtained assuming that the densities of the target and projectile remain constant and equal to their respective ground

[2]Although this theory has been called improperly TDHF in the past, we will continue to use this acronym in this work.

state densities. This leads to the so-called *frozen density* (FD) approximation (see, for instance, Ref. [45]). In this limit, the interaction potential between a target and projectile with their ground state densities denoted, respectively, by $\hat{\rho}_T$ and $\hat{\rho}_P$ reads

$$V^{\rm FD}(R) = \mathcal{E}[\hat{\rho}_{P+T}](R) - \mathcal{E}[\hat{\rho}_T] - \mathcal{E}[\hat{\rho}_P], \qquad (2)$$

where $\hat{\rho}_{P+T} = \hat{\rho}_P + \hat{\rho}_T$ is the total density obtained by summing the densities of the target and projectile assuming that their centers of mass are at a given relative distance R. Note that $\mathcal{E}[\hat{\rho}_{P+T}]$ here neglects the Pauli effect by the two overlapping densities. As we will see in the following, we use the property of the extracted potentials with the FD technique essentially at the Coulomb barrier. At this point, overlap of the two densities is small, and Pauli effect is expected to be accordingly small. It should, however, be kept in mind that a proper account of the Pauli principle would lead to an increase of the potential for small relative distances.

D. Matching TDHF with a two-body collision problem

The FD approximation is expected to break down if strong reorganization of internal one-body degrees of freedom occurs in the approaching phase. In the following, methods of extracting the nucleus-nucleus potential directly from TDHF without assuming frozen densities are discussed.

1. Definition of the separation plane

The first step is to properly define the collective coordinate R that separates the two subsystems. Here, we follow macroscopic models and define the plane of separation at the neck position. In practice, the neck position is obtained by considering the two densities

$$\rho_{T,P}(\mathbf{r}, t) = \sum_{n \in T,P} \left|\varphi_n^{T,P}(\mathbf{r}, t)\right|^2,$$

where $\varphi_n^T(\mathbf{r}, t)$ and $\varphi_n^P(\mathbf{r}, t)$ denote single-particle wave functions initially in, respectively, the target and projectile, which are propagated in the mean field of the composite system up to time t. Note that if the approaching phase is fast enough, these densities have no time to evolve and are expected to be very close to their respective ground state densities. The separation plane at a given time t is then defined at the position where isocontours of the two densities $\rho_T(\mathbf{r}, t)$ and $\rho_P(\mathbf{r}, t)$ cross. An example of densities $\rho_{P,T}(\mathbf{r})$ (solid lines) as well as the deduced separation plane (vertical thick line) is given for the reaction $^{16}\mathrm{O} + ^{208}\mathrm{Pb}$ in bottom of Fig. 1. This figure illustrates that the separation plane corresponds to the geometrical neck as generally defined in leptodermous systems.

2. Two-body kinematics

Once the separation plane is defined, all quantities relative to the dynamics of the two subsystems can be calculated. We associate to each subspace an index $i = 1, 2$ and a density $\hat{\rho}_i(t)$, which equals the total density in the subspace i and cancels out in the opposite side of the separation plane. Then, all quantities of interest could be computed as the number of nucleons in each side of the separation plane, i.e., $A_i(t) \equiv \mathrm{Tr}(\hat{\rho}_i(t))$. Since we are considering head-on collisions along the x axis, the c.m. coordinate $R_i(t)$ and associated momentum $P_i(t)$ are expressed as

$$R_i(t) \equiv \mathrm{Tr}(\hat{x}\,\hat{\rho}_i(t))/A_i(t), \qquad P_i(t) \equiv \mathrm{Tr}(\hat{p}_x\hat{\rho}_i(t)). \qquad (3)$$

We can also compute the inertial mass of the two subsystems, denoted by m_i, from the TDHF evolution using $m_i = P_i/\dot{R}_i$. Once these quantities are obtained, the TDHF dynamics can be reduced to the two-body collision problem, where the relative distance $R(t) = R_1 - R_2$, associated momentum $P(t) = (m_2P_1 - m_1P_2)/(m_1 + m_2)$, and reduced mass

$$\mu = \frac{m_1 m_2}{m_1 + m_2}, \qquad (4)$$

are computed at each time step. Note that when the two nuclei are far from each other, the reduced mass properly identifies with its initial value $\mu_{\rm ini} = mA_TA_P/(A_T + A_P)$, where A_T and A_P denote, respectively, the initial target and projectile mass numbers,[3] and m is the nucleon mass. It is worth mentioning that whereas for symmetric reactions μ remains constant during the collision, for the asymmetric case μ may vary after the contact, i.e., $\mu = \mu(R)$. The critical discussion on the possible influence of this variation on extracted potentials is presented in Sec. III E.

E. Dynamical effects on nucleus-nucleus potentials

The violation of the FD prescription might at least be assigned to two effects. (i) In TDHF, the total one-body density $\hat{\rho}(t)$ does evolve in time. Therefore, the frozen density used in Eq. (2) should *a priori* be replaced by the density reached dynamically during the evolution to get a more realistic nucleus-nucleus potential from the TDHF. (ii) A second crucial aspect is that part of the relative kinetic energy is transformed into internal excitations. This effect is generally treated as a dissipative process in macroscopic theories.

To include effect (i) and extract interaction potentials that account for the possible evolution of the density along the TDHF path, the so-called density-constrained TDHF (DC-TDHF) technique has been developed [41,42,49]. In this method, at each time step, $\rho(\mathbf{r}, t)$ is deduced from TDHF. Then, the EDF is minimized under the constraint that the total density matches $\rho(\mathbf{r}, t)$. Denoting the minimized energy by $\mathcal{E}_{\rm DC}[\hat{\rho}(t)](R)$, the potential is then given by

$$V^{\rm DC}(R) = \mathcal{E}_{\rm DC}[\hat{\rho}(t)](R) - \mathcal{E}[\hat{\rho}_T] - \mathcal{E}[\hat{\rho}_P]. \qquad (5)$$

The great interest of the DC-TDHF method lies in the ability to access the adiabatic potential accounting for realistic density profiles.

[3] The discrepancy on the reduced mass found here very close to $\mu(R)/\mu_{\rm ini} \simeq 1$ and the one around 0.67 in Ref. [33] was due to time-odd terms of the Skyrme field which were not properly computed in the original version of the 3D code [31]. This problem is now fixed.

F. Matching TDHF with binary dissipative collisions

An alternative technique proposed in Ref. [29] and preliminarily tested in Ref. [33] consists of assuming that the time evolution of R and its canonical momentum P obey a classical equation of motion including a friction term that depends on the velocity $\dot{R}$:

$$\frac{dR}{dt} = \frac{P}{\mu(R)},$$
$$\frac{dP}{dt} = -\frac{dV^{\mathrm{DD}}}{dR} + \frac{1}{2}\frac{d\mu(R)}{dR}\dot{R}^2 - \gamma(R)\dot{R}, \tag{6}$$

where $V^{\mathrm{DD}}(R)$ and $\gamma(R)$ denote, respectively, the nucleus-nucleus potential and friction coefficient (here DD stands for dissipative dynamics). The friction coefficient $\gamma(R)$ describes the effect of energy dissipation from the macroscopic degrees of freedom to the microscopic ones. This method is of great interest because it offers the possibility of accessing interaction potentials that account for possible dynamical effects and obtaining information on the dissipative process from a fully microscopic theory. In the following, we show that this method is a valuable tool.

1. Discussion on the R-dependent mass

Before presenting applications, additional remarks on the origin of the $d\mu(R)/dR$ term in Eq. (6) are mandatory. To obtain the equation, we implicitly assume that the total energy can be written as a sum of a Hamiltonian part and a dissipative part E_{diss}, i.e.,

$$E = \frac{P^2}{2\mu(R)} + V^{\mathrm{DD}}(R) + E_{\mathrm{diss}}, \tag{7}$$

where the reduced mass depends explicitly on R. For canonical variables (R, P), the Hamilton part in Eq. (6) arises from the derivative of the kinetic and V^{DD} part in the previous equation. Using $\frac{1}{2}\frac{d\mu(R)}{dR}\dot{R}^2 = -\frac{d}{dR}(\frac{P^2}{2\mu(R)})$, we finally obtain the second equation in Eq. (6). The appearance of the R-dependent reduced mass in dynamical mean-field calculations has been reported in Refs. [33,42] and turned out to be weak before the Coulomb barrier. In all applications presented below, we explicitly neglected the second term in the evolution of P. Indeed, including it or not or taking directly $\mu(R) = \mu_{\mathrm{ini}}$ has no effect on the barrier height and position presented in this work. For the sake of completeness, this aspect is illustrated in Sec. III E.

III. APPLICATION

A. Procedure to obtain $V^{\mathrm{DD}}(R)$ and $\gamma(R)$

In Eq. (6), we have three unknown quantities: the reduced mass $\mu(R)$ entering in the first equation, the friction coefficient $\gamma(R)$, and the nucleus-nucleus potential $V^{\mathrm{DD}}(R)$ appearing in the relative momentum evolution. The reduced mass can be directly deduced from a single TDHF trajectory. Indeed, both $R(t)$ and $P(t)$ can be computed at all time along the mean-field trajectory. From $R(t)$, $\dot{R}(t)$ is simply computed from

$$\dot{R}(t) \equiv \frac{R(t+\Delta t) - R(t-\Delta t)}{2\Delta t}, \tag{8}$$

where Δt corresponds to the numerical time step used in TDHF. We finally deduced $\mu(R)$ from $P(t)/\dot{R}(t)$.

To obtain the two remaining unknown quantities $\gamma(R)$ and $V^{\mathrm{DD}}(R)$, a single TDHF trajectory is not sufficient. We assume that the potential energy and the friction parameter are not affected by a slight change in c.m. energy and consider two head-on collisions with energies $E_{\mathrm{I}} = E_{\mathrm{c.m.}}$ and $E_{\mathrm{II}} = E_{\mathrm{c.m.}} + \Delta E$ (in practice $\Delta E/E_{\mathrm{c.m.}} \simeq 1 - 2\%$ is used). A couple of canonical variables $(R_{\mathrm{I/II}}, P_{\mathrm{I/II}})$ is associated to each trajectory. Assuming that Eq. (6) applies in both cases with the same potential and friction, we deduce that

$$\gamma(R) = -\frac{[\dot{P}_{\mathrm{I}}]_{R_{\mathrm{I}}=R} - [\dot{P}_{\mathrm{II}}]_{R_{\mathrm{II}}=R}}{[\dot{R}_{\mathrm{I}}]_{R_{\mathrm{I}}=R} - [\dot{R}_{\mathrm{II}}]_{R_{\mathrm{II}}=R}}. \tag{9}$$

Then, using one of the trajectories, we obtain dV^{DD}/dR as a function of relative distance. The potential $V^{\mathrm{DD}}(R)$ is deduced by integration over R using its asymptotic Coulomb potential at large relative distances. The present method clearly relies on the hypothesis that the mean-field dynamics could properly be reduced to a one-dimensional macroscopic description. As we will see, this potential compares rather well with other techniques validating *a posteriori* the macroscopic reduction used in this work. Finally, $V^{\mathrm{DD}}(R)$ is also expected to contain dynamical effects such as density evolution.

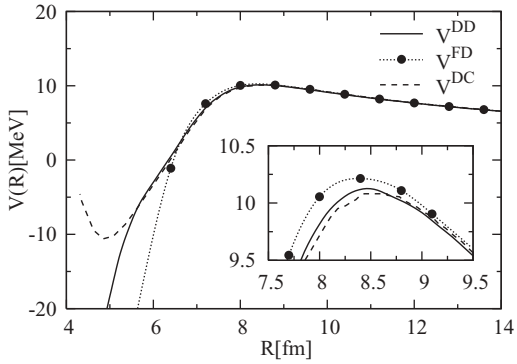

FIG. 2. Comparison of potential energies for the ^{16}O+^{16}O reaction obtained from the different models. The solid, dashed, and filled circles-dotted line correspond to the DD-TDHF, DC-TDHF [41], and FD potentials, respectively. A zoom on the Coulomb barrier region is also shown in the insert.

B. Illustrative example: ^{16}O+^{16}O

The potential $V^{\mathrm{DD}}(R)$ obtained with the dissipative dynamics reduction method for the $^{16}\mathrm{O} + {}^{16}\mathrm{O}$ reaction at $E_{\mathrm{c.m.}} = 34$ MeV (and $\Delta E = 1$ MeV) is displayed in Fig 2. The DC-TDHF potential obtained in Ref. [41][4] and the

[4]Note, however, that a different set of parameters was used for the Skyrme effective interaction and numerical aspects.

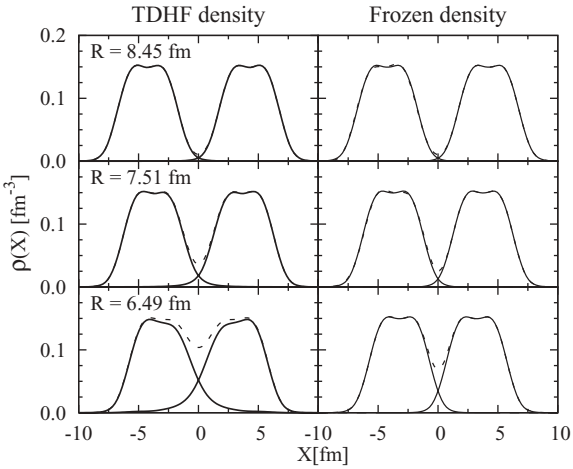

FIG. 3. Left: Density profiles $\rho(X,0,0)$ (dashed) and $\rho_{P/T}(t)$ (solid lines) obtained with TDHF for the head-on $^{16}O+^{16}O$ collision at $E_{\text{c.m.}}=34$ MeV at three different times. Each value of relative distance R is indicated in each left panel. Right: Densities $\rho(X,0,0)$ (dashed lines) obtained at the same relative distances within the FD approximation. In this case, $\rho_{P/T}(X,0,0)$ (solid lines) identify with the ground state densities of the ^{16}O nucleus.

FD potential are also displayed for comparison. Figure 2 shows that potentials extracted from the DD- and DC-TDHF methods are very close to each other (almost identical) even well inside the Coulomb barrier (up to $R=5.3$ fm). The fact that the potential deduced from our method matches the DC-TDHF result gives us confidence in the specific macroscopic equation [Eq. (6)] retained to reduce the microscopic dynamics. In addition, both methods are almost identical to the FD description (for $R\geqslant 6.5$ fm). This indicates that little reorganization of densities occurs in the approaching phase. This is indeed confirmed in Fig. 3, where the TDHF density profiles obtained at different relative distances are directly compared with densities used in the FD approximation for the same R. At and below the estimated barrier radius $R_B=8.46$ fm, little difference between the densities $\rho_{P/T}(X,0,0)$ (left, solid line) and the ground state densities (right, solid line) can be seen. As a consequence, the Coulomb barrier predicted by TDHF is almost identical to the one obtained in the FD case (the difference being less than 0.1 MeV). It is worth mentioning at this point that our method assumes neither sudden nor adiabatic approximation. Another conclusion that could be drawn from the matching between DD-TDHF or DC-TDHF and the FD approximation is that Pauli blocking effects, which are automatically incorporated in the two former approaches and partially neglected in V^{FD}, do not seem to play a significant role close to the Coulomb barrier in $^{16}O+^{16}O$.

Figure 2 indicates that dynamical effects marginally affect the potential felt by the two partners in the approaching phase. In the next section, we will indeed see that similar conclusions hold in most cases studied when $E_{\text{c.m.}}$ is well above the Coulomb barrier. This is the case presented here where $E_{\text{c.m.}}$ is three times more than the Coulomb barrier. In this limit, the spatial organization of nucleons inside each nucleus is almost frozen before the contact.

C. Systematic study of nucleus-nucleus potential at high c.m. energy

The previous study is extended to fusion reactions with various combinations of nuclei. Since deformed nuclei have orientations with respect to the collision axis, which increases the macroscopic degrees of freedom to be considered, we concentrate on collisions involving spherical nuclei. The DD-TDHF technique is applied to the systems $^{40}Ca+^{40}Ca$ and $^{48}Ca+^{48}Ca$ for mass symmetric reactions and $^{16}O+^{40,48}Ca$, $^{40}Ca+^{48}Ca$, $^{16}O+^{208}Pb$, and $^{40}Ca+^{90}Zr$ for mass asymmetric reactions.

In all systems, we do expect that when the c.m. energy increases, the potential will identify with the FD case. We have checked that this is indeed the case and identified the minimum energy for which the FD limit is reached. Potentials obtained with the DD-TDHF are displayed by the solid lines in Fig. 4 and are systematically compared with the FD approximation. In Figs. 4(a) and 4(b), the c.m. energy used to perform the macroscopic reduction is about two times the Coulomb barrier energy. Similar to the $^{16}O+^{16}O$ reaction case, all the examples presented in Figs. 4(a) and 4(b) follow closely the FD approximation. Higher c.m. energies have to be used to reach the FD case in the systems presented in Figs. 4(c) and 4(d). We report in Fig. 5 the c.m. energy threshold, denoted by $E^{\text{FD}}_{\text{c.m.}}$, which corresponds to the minimal $E_{\text{c.m.}}$ for which the DD-TDHF method gives the FD results (within 5% in general) as a function of the FD barrier. The different Coulomb barrier energies deduced from the DD-TDHF method applied at high c.m. energies [denoted as V_B^{DD} (high $E_{\text{c.m.}}$)] are reported in Table I. These barriers are systematically compared with the FD case and experimental data taken from Refs. [15,58,59]. Overall, we see that the DD-TDHF method applied at high c.m. energy gives a qualitative agreement with experiments. It is noticeable, however, that the barrier height is systematically higher than the experimental observation and that the discrepancy increases as $Z_P Z_T$ increases.

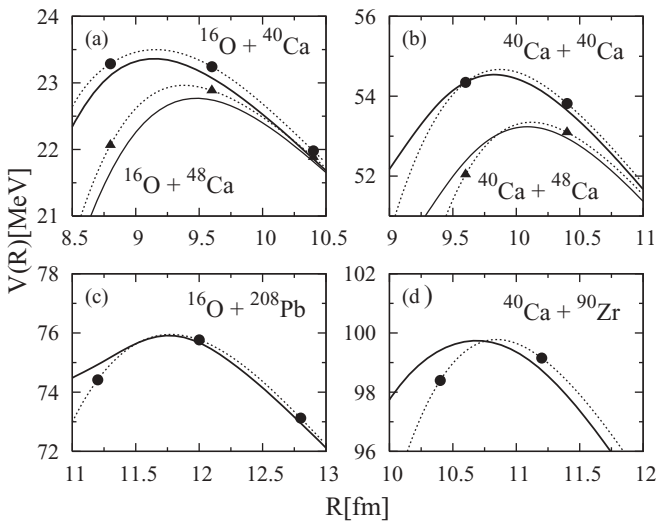

FIG. 4. Potentials extracted from the DD-TDHF (solid lines) at high c.m. energies compared with V^{FD} (filled circles- and triangles-dotted lines).

TABLE I. Energy (in MeV) and radii (in fm) of the Coulomb barrier extracted from the DD-TDHF method. V_B^{DD} (high $E_{c.m.}$) refers to the barrier deduced for $E_{c.m.} > E_{c.m.}^{FD}$, while V_B^{DD} (low $E_{c.m.}$) corresponds to the lowest Coulomb barrier deduced from TDHF using $E_{c.m.} \simeq V_B^{FD}$. Available experimental values taken from Refs. [15,58,59] are also reported.

Reaction	V_B^{FD}	V_B^{DD} (high $E_{c.m.}$)	V_B^{DD} (low $E_{c.m.}$)	V_B^{exp}	R_B^{FD}	R_B^{DD} (high $E_{c.m.}$)	R_B^{DD} (low $E_{c.m.}$)	R_B^{exp}
$^{16}O+^{16}O$	10.2	10.13	10.12	10.61 [58]	8.4	8.46	8.52	7.91 [58]
$^{16}O+^{40}Ca$	23.5	23.36	23.07	23.06 [58]	9.2	9.18	9.50	9.21 [58]
$^{16}O+^{48}Ca$	23.0	22.77	22.48		9.4	9.50	9.75	
$^{40}Ca+^{40}Ca$	54.7	54.54	53.35	52.8 [15]	9.8	9.82	10.32	
$^{40}Ca+^{48}Ca$	53.4	53.24	52.13	52.00 [59]	10.1	10.09	10.56	9.99 [59]
$^{48}Ca+^{48}Ca$	52.4	52.13	50.97	51.49 [59]	10.3	10.38	10.82	10.16 [59]
$^{16}O+^{208}Pb$	76.0	75.91	74.51	74.52 [59]	11.8	11.74	12.14	11.31 [59]
$^{40}Ca+^{90}Zr$	99.8	99.98	97.71	96.88 [59]	10.8	10.63	11.27	10.53 [59]

We will see in the following that part of the difference observed could be understood in terms of departure from the FD limit as the c.m. energy approaches the Coulomb barrier. Indeed, as the energy decreases, densities have more time to reorganize.

D. C.m. energy dependence of nucleus-nucleus potential close to the Coulomb barrier

In the previous examples, we determined the typical c.m. energy above which the potential deduced from the DD-TDHF technique corresponds to the FD case. Here, we show that the extracted potential energy is slightly modified as the c.m. energy decreases and approaches the Coulomb barrier. As shown below, this energy dependence of the nucleus-nucleus potentials underlines the role of dynamical effects.

1. Dynamical reduction of the Coulomb barrier energy

To illustrate the c.m. energy dependence of the potential, Fig. 6 presents potentials obtained with the DD-TDHF method using several c.m. energies ranging from $E_{c.m.} = 55$ to 100 MeV for the $^{40}Ca + ^{40}Ca$ reaction. Again, in the high-energy limit, potentials identify with the FD case. In addition, an increase of c.m. energy from $E_{c.m.} = 90$ to 100 MeV leads to identical results, indicating the stability of the method as the energy increases. In contrast, as $E_{c.m.}$ decreases, potentials deduced from the DD-TDHF deviate from the FD case. As $E_{c.m.}$ approaches the Coulomb barrier energy, a small change in $E_{c.m.}$ significantly affects V^{DD} as illustrated by the two energies $E_{c.m.} = 55$ and 57 MeV displayed in Fig. 6. To quantify this dependence, we have reported in Fig. 7 values of the Coulomb barrier, V_B^{DD}, deduced from the DD-TDHF method as a function of c.m. energy. Again, if $E_{c.m.}$ is high, V_B^{DD} becomes very close to the FD case. As $E_{c.m.}$ decreases, V_B^{DD} is more and more reduced compared to V_B^{FD}. This effect, observed in all the cases considered here and called hereafter the "dynamical barrier reduction," is a direct consequence of reorganization of densities in the approaching phase. This is clearly illustrated in Fig. 8, where density profiles obtained for the $^{40}Ca + ^{40}Ca$ reaction at three c.m. energies ($E_{c.m.} = 55$, 57, and 90 MeV are shown from top to bottom, respectively) and for specific R values. In Fig. 8, only the case of $E_{c.m.} =$ 90 MeV resembles the FD case. At lower energies, a clear deviation from the FD density profile is observed. Considering $E_{c.m.} = 55$ MeV, as the two partners approach, deformation of the two nuclei takes place. This deformation initiates the formation of a neck at larger relative distances compared to $E_{c.m.} = 90$ MeV. The c.m. energy dependence of the potential extracted with the DD-TDHF technique reflects the difference in the density profiles accessed dynamically during

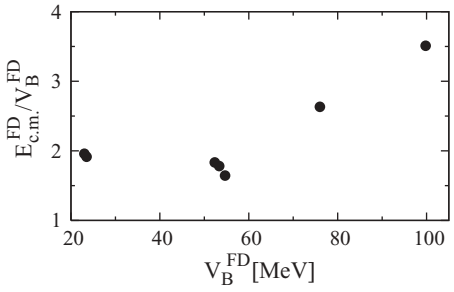

FIG. 5. Minimal c.m. energy $E_{c.m.}^{FD}$ for which the potentials deduced from the DD-TDHF method identify with the FD case. This quantity is presented as a function of the FD barrier energy.

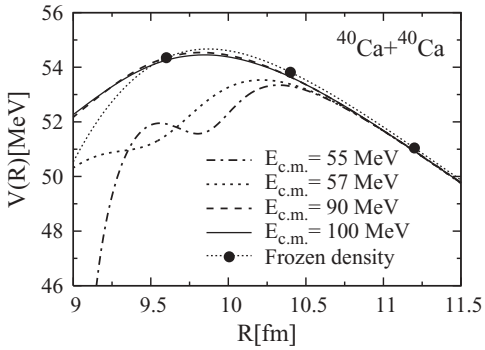

FIG. 6. Potential energy for the $^{40}Ca + ^{40}Ca$ reaction extracted at different c.m. energies. The FD potential is displayed with the filled circles-dotted line.

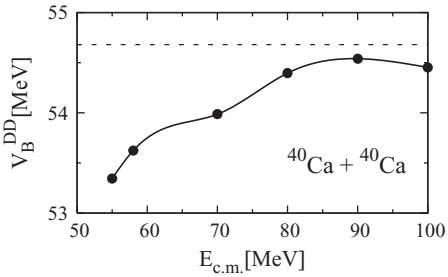

FIG. 7. Barrier energy V_B^{DD} for the $^{40}Ca + ^{40}Ca$ reaction extracted at different c.m. energies. The horizontal dashed line indicates the FD reference.

the mean-field evolution. Note that a similar dependence is *a priori* also expected in the DC-TDHF method [41,42], which accounts for the dynamical deformation of the densities.

In all cases considered in this work, a reduction of the "apparent" Coulomb barrier seen by the two nuclei before fusion is observed compared to the FD case. This reduction could always be assigned to large density deformation close to the barrier. To quantify the magnitude of the dynamical reduction effect, we have systematically extracted the lowest barrier energy. This quantity [denoted as V_B^{DD} (low $E_{c.m.}$)], reported in the third column of Table I, is obtained when the c.m. energy used in DD-TDHF equals the corresponding V_B^{FD}. In Fig. 9, the difference between the lowest barrier and the FD barrier is displayed as a function of V_B^{FD}. We see that the difference increases almost linearly with V_B^{FD}, i.e., with the initial $Z_P Z_T$. As mentioned previously, the Coulomb barrier energy obtained within the FD approximation generally overestimates the Coulomb barrier energy deduced from experiments (see Table I). The discrepancy increases as $Z_P Z_T$ increases. Interestingly enough, the lowest energy V_B^{DD} is much closer to the experimental observation, particularly for large $Z_P Z_T$.

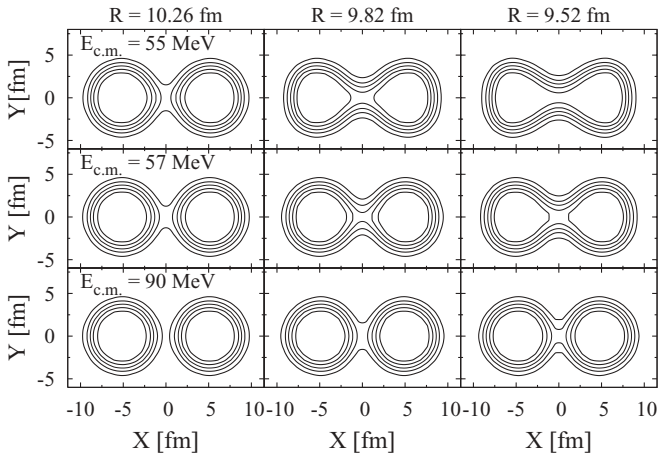

FIG. 8. Density profiles obtained in TDHF for different relative distances R for the $^{40}Ca + ^{40}Ca$ reaction at three different c.m. energies. These energies correspond to those used in Fig. 7 to obtain $V^{DD}(R)$.

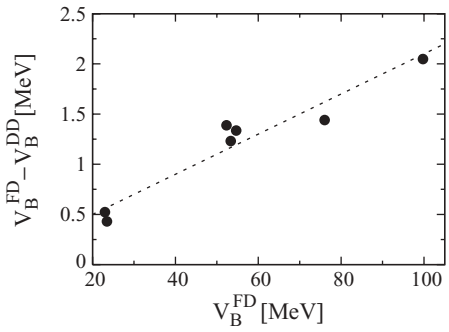

FIG. 9. Difference between the barrier obtained with the FD approximation and the lowest barrier with DD-TDHF as a function of V_B^{FD}. In practice, the lowest barrier is obtained by using c.m. energy at or close to V_B^{FD}.

2. *Critical discussion on the one-dimensional reduction: The* $^{16}O + ^{208}Pb$ *case*

Previous discussions point out that various density profiles might be accessed depending on the c.m. energy used in the TDHF. In macroscopic models, such a diversity in densities is usually accounted for by considering the multidimensional collective space where the deformation and/or neck are explicitly treated as relevant variables [1–5]. Therefore, the energy dependence of the potential deduced with the DD-TDHF method should *a priori* be understood as different paths in a more complex multidimensional potential energy landscape. As a consequence, one should also *a priori* consider the macroscopic reduction of TDHF with additional collective degrees of freedom, which might become extremely complicated.

Here, we show that the simple one-dimensional macroscopic reduction still contains meaningful information on the fusion process. We consider the $^{16}O + ^{208}Pb$ reaction for which extensive TDHF calculations have been performed [36,60].

Different potentials deduced for this reaction using the DD-TDHF method with different c.m. energies are displayed in Fig. 10. A more complex energy dependence is observed in this case than for the $^{40}Ca + ^{40}Ca$ reaction displayed in Fig. 6. In particular, at intermediate c.m. energies ($100 < E_{c.m.} < 200$ MeV), the nucleus-nucleus potential is above the FD case. This is clearly illustrated in Fig. 11, where the

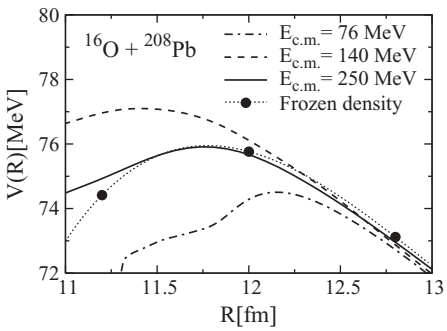

FIG. 10. Potential energy obtained with the DD-TDHF method for the $^{16}O + ^{208}Pb$ reaction using different c.m. energies. The filled circles correspond to the FD approximation.

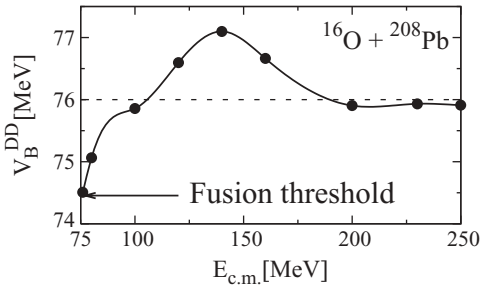

FIG. 11. Coulomb barrier energy V_B^{DD} for the $^{16}O + ^{208}Pb$ reaction as a function of the c.m. energy. The horizontal dashed line indicates the FD reference; the arrow indicates the low-energy fusion TDHF threshold obtained with TDHF calculations in Ref. [36].

Coulomb barrier energy V_B^{DD} is shown as a function of $E_{c.m.}$. A bump for intermediate c.m. energies is clearly seen. Note that a similar behavior is also observed in the $^{40}Ca + ^{90}Zr$ case, indicating that the energy dependence might be more complex as $Z_P Z_T$ increases. However, in view of the potential change compared to the c.m. energy involved (almost two times V_D^{FD}), this bump is not expected to change drastically the fusion probability obtained with TDHF. In contrast, when the c.m. energy is close to the Coulomb barrier, a small change in the potential will modify significantly the fusion probability. In the following, we will concentrate on this region.

The low-energy fusion TDHF threshold, which is defined as the minimum c.m. energy required to fusion in TDHF, is indicated by an arrow in Fig. 11. A very precise value of 74.45 MeV was obtained for this threshold in Ref. [36] using the same TDHF code with the SLy4d Skyrme effective interaction by performing a large number of TDHF calculations. The lowest barrier energy obtained with the DD-TDHF method perfectly matches this threshold. Again, this gives additional confidence in this method to provide precise information on the nucleus-nucleus potential extracted.

E. Effect of coordinate-dependent mass

In previous sections, the macroscopic equation (6) without the term $\frac{1}{2}\frac{d\mu(R)}{dR}\dot{R}^2$ was used as a starting point for extracting potentials from the DD-TDHF method. This equation is *a priori* only valid for systems with constant reduced mass. This condition is exactly fulfilled by the mean-field evolution for symmetric collisions. For asymmetric reactions, dependence of the reduced mass with relative distance is possible. This situation is illustrated in Fig. 12, where the reduced mass estimated through Eq. (4) divided by its initial value μ_{ini} is shown as a function of R/R_B^{FD}. In all cases, a deviation from the initial value is observed. In particular, this deviation might be significant for the most asymmetric case, $^{16}O + ^{208}Pb$, at small relative distances. Similar behavior has been discussed in Ref. [42]. In all cases, the c.m. energy used in the calculation corresponds to V_B^{FD} (see Table I).

To estimate the possible effect of the R-dependent reduced mass on the extracted potential and friction coefficient, we also extracted potentials and friction coefficients from Eq. (6) including the term $\frac{1}{2}\frac{d\mu(R)}{dR}\dot{R}^2$. Using the same procedure as

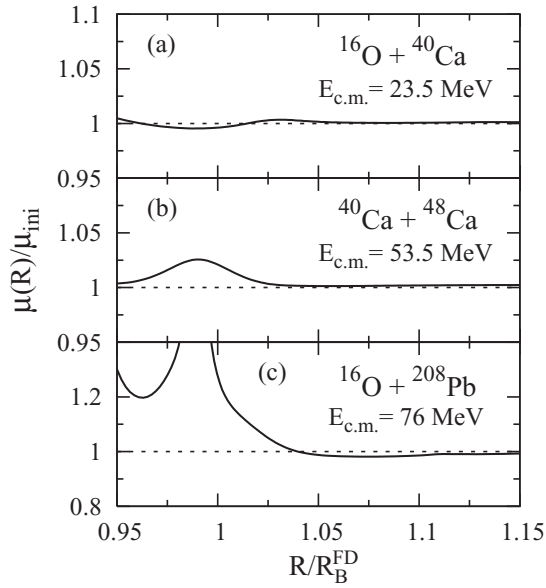

FIG. 12. Reduced mass deduced from the procedure described in Sec. III A divided by its initial value μ_{ini} as a function of relative distance divided by the Coulomb barrier radius for the FD case (R_B^{FD}) for the three mass-asymmetric reactions. The c.m. energies used are reported in each panel.

described in Sec. III A, a new potential V^{DD} can be extracted. In Fig. 13, potentials with (solid lines) and without (filled triangles) this term are compared for the mass-asymmetric $^{16}O+^{40}Ca$, $^{40}Ca+^{48}Ca$, and $^{16}O + ^{208}Pb$ reactions. In the first

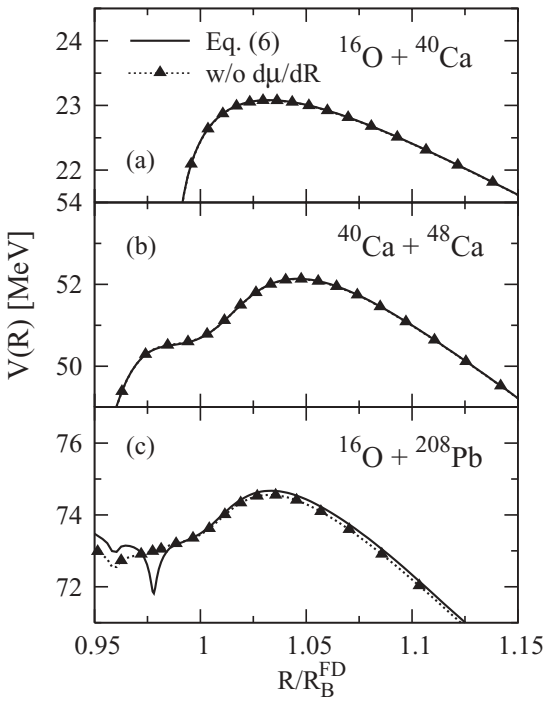

FIG. 13. Comparison of potentials extracted from Eq. (6) (solid line) and from Eq. (6) without the term $\frac{1}{2}\frac{d\mu(R)}{dR}\dot{R}^2$ (filled triangles-dotted line) as a function of R/R_B^{FD}. The c.m. energies used are the same as in Fig. 12.

two cases, the two potentials are indistinguishable, while in the last case a small difference between the two potentials is observed. Though we see from Fig. 12 that the reduced mass depends on the relative distance, Fig. 13 shows that this dependence has almost no effect on the nucleus-nucleus potential extracted with the DD-TDHF method.

IV. SUMMARY

The first goal of the present paper was to benchmark a technique, called DD-TDHF, to obtain nucleus-nucleus potentials and dissipation using a macroscopic reduction of mean-field theory based on Eq. (6). Several results have been obtained that validate the DD-TDHF technique. (i) Used with the same conditions, the DD-TDHF method leads to a potential very close to the DC-TDHF result [41] (Fig. 2). (ii) As expected, using high c.m. energies, the DD-TDHF method converges toward the FD approximation (Fig. 4). (iii) At c.m. energy close to the Coulomb barrier energy, the dynamical reduction of the barrier found with the DD-TDHF is able to reproduce the low-energy TDHF fusion threshold obtained in Ref. [36] for $^{16}O + ^{208}Pb$ (Fig. 11). Nucleus-nucleus potentials obtained with the DD-TDHF method automatically incorporate dynamical effects during the approaching phase which could be traced back in the energy dependence of the nucleus-nucleus potential. This energy dependence has been systematically investigated for the mass symmetric reactions $^{16}O + ^{16}O$, $^{40}Ca + ^{40}Ca$, and $^{48}Ca + ^{48}Ca$ and mass asymmetric systems $^{16}O + ^{40,48}Ca$, $^{16}O + ^{208}Pb$, $^{40}Ca + ^{48}Ca$, and $^{40}Ca + ^{90}Zr$. For this systematic, the following aspects have been discussed:

(i) We show that in all reactions the minimal energy ($E^{FD}_{c.m.}$) for which the FD potential is recovered with the DD-TDHF can always be identified. This energy has been systematically investigated. We have shown that $E^{FD}_{c.m.}/V^{FD}_{B}$ increases as the $Z_P Z_T$ increases (Fig. 5).

(ii) A clear energy dependence of extracted potential, due to dynamical effects that modify the density profile, has been observed in all cases. For systems with $Z_P Z_T \leqslant 400$, a continuous decrease of the apparent Coulomb barrier is seen as the c.m. energy decreases (Fig. 7), while in other systems ($^{16}O + ^{208}Pb$ and $^{40}Ca + ^{90}Zr$) more complex energy dependence of the Coulomb barrier energy is obtained (Fig. 11).

(iii) In all cases, the nucleus-nucleus potential deduced from the DD-TDHF method varies rapidly as the c.m. energy approaches the Coulomb barrier energy. Such a rapid change could be assigned to the difference in density profiles dynamically obtained in various TDHF calculations performed with slightly different $E_{c.m.}$.

(iv) Dynamical effects reduce the apparent barrier below that of the FD case by 2–3% of V^{FD}_{B} (Fig. 9). While the FD Coulomb barrier generally overestimates the Coulomb barrier estimated experimentally, barriers including the dynamical reduction effect become very close to the experimental case (Table I).

In summary, the DD-TDHF method has been successfully tested in the present work. It gives interesting insight into the nucleus-nucleus potentials that account for dynamical effects. Mean-field calculations show energy dependence close to the Coulomb barrier energy. Such energy dependence is also expected to affect the subbarrier fusion process. Unfortunately, TDHF does not provide a correct description of tunneling in collective space. The study of subbarrier fusion with mean-field theory would be very interesting but clearly requires to go beyond TDHF. Finally, we would like to mention that the DD-TDHF technique also gives dissipative kernels from a fully microscopic theory. This aspect, which is crucial in macroscopic theory, will be discussed in a forthcoming article [57].

ACKNOWLEDGMENTS

We thank P. Bonche for providing the 3D TDHF code and S. Ayik, B. Avez, D. Boilley, C. Simenel, and B. Yilmaz for fruitful discussions. K.W. was supported by research grants from the Japan Society for the Promotion of Science for Young Scientists and acknowledges GANIL for its warm hospitality.

[1] W. Nörenberg and H. A. Weidenmüller, *Introduction to the Theory of Heavy-Ion Collisions* (Springer-Verlag, Berlin, 1976).
[2] R. W. Hasse and W. D. Myers, *Geometrical Relationships of Macroscopic Nuclear Physics* (Springer-Verlag, Berlin, 1988).
[3] R. A. Broglia and A. Winther, *Heavy Ion Reactions* (Addison-Wesley, Redwood City, CA, 1991).
[4] W. Reisdorf, J. Phys. G **20**, 1297 (1994).
[5] P. Fröbrich and R. Lipperheide, *Theory of Nuclear Reactions* (Oxford University Press, New York, 1996).
[6] R. Bass, Nucl. Phys. **A231**, 45 (1974); *Nuclear Reactions with Heavy Ions* (Springer-Verlag, New York, 1980).
[7] J. Blocki, J. Randrup, W. J. Swiatecki, and C. F. Tsang, Ann. Phys. (NY) **105**, 427 (1977).
[8] W. D. Myers and W. J. Swiatecki, Phys. Rev. C **62**, 044610 (2000).
[9] H. J. Krappe, J. R. Nix, and A. J. Sierk, Phys. Rev. C **20**, 992 (1979).
[10] G. Satchler and W. Love, Phys. Rep. **55**, 183 (1979).
[11] P. Möller and A. Iwamoto, Nucl. Phys. **A575**, 381 (1994).
[12] T. Ichikawa, A. Iwamoto, P. Möller, and A. J. Sierk, Phys. Rev. C **71**, 044608 (2005).
[13] C. H. Dasso, S. Landowne, and A. Winther, Nucl. Phys. **A405**, 381 (1983); **A407**, 221 (1983).
[14] A. B. Balantekin and N. Takigawa, Rev. Mod. Phys. **70**, 77 (1998).
[15] M. Dasgupta, D. J. Hinde, N. Rowley, and A. M. Stefanini, Annu. Rev. Nucl. Part. Sci. **48**, 401 (1998).
[16] C. L. Jiang *et al.*, Phys. Rev. Lett. **89**, 052701 (2002).
[17] C. L. Jiang *et al.*, Phys. Rev. Lett. **93**, 012701 (2004).
[18] C. L. Jiang *et al.*, Phys. Rev. C **71**, 044613 (2005).
[19] C. L. Jiang, B. B. Back, H. Esbensen, R. V. F. Janssens, and K. E. Rehm, Phys. Rev. C **73**, 014613 (2006).

[20] M. Dasgupta, D. J. Hinde, A. Diaz-Torres, B. Bouriquet, C. I. Low, G. J. Milburn, and J. O. Newton, Phys. Rev. Lett. **99**, 192701 (2007).
[21] S. Misicu and H. Esbensen, Phys. Rev. Lett. **96**, 112701 (2006); Phys. Rev. C **75**, 034606 (2007).
[22] H. Esbensen and S. Misicu, Phys. Rev. C **76**, 054609 (2007).
[23] T. Ichikawa, K. Hagino, and A. Iwamoto, Phys. Rev. C **75**, 057603 (2007).
[24] P. Bonche, S. E. Koonin, and J. W. Negele, Phys. Rev. C **13**, 1226 (1976).
[25] S. E. Koonin, K. T. R. Davies, V. Maruhn-Rezwani, H. Feldmeier, S. J. Krieger, and J. W. Negele, Phys. Rev. C **15**, 1359 (1977).
[26] H. Flocard, S. E. Koonin, and M. S. Weiss, Phys. Rev. C **17**, 1682 (1978).
[27] P. Bonche, B. Grammaticos, and S. E. Koonin, Phys. Rev. C **17**, 1700 (1978).
[28] R. Y. Cusson, J. A. Maruhn, and H. W. Meldner, Phys. Rev. C **18**, 2589 (1978).
[29] S. E. Koonin, Prog. Part. Nucl. Phys. **4**, 283 (1980).
[30] J. W. Negele, Rev. Mod. Phys. **54**, 913 (1982).
[31] K.-H. Kim, T. Otsuka, and P. Bonche, J. Phys. G **23**, 1267 (1997).
[32] C. Simenel, Ph. Chomaz, and G. de France, Phys. Rev. Lett. **86**, 2971 (2001).
[33] D. Lacroix, arXiv:nucl-th/0202063.
[34] C. Simenel and Ph. Chomaz, Phys. Rev. C **68**, 024302 (2003).
[35] C. Simenel, Ph. Chomaz, and G. de France, Phys. Rev. C **76**, 024609 (2007).
[36] C. Simenel and B. Avez, Int. J. Mod. Phys. E **17**, 31 (2008).
[37] T. Nakatsukasa and K. Yabana, Phys. Rev. C **71**, 024301 (2005).
[38] J. A. Maruhn, P.-G. Reinhard, P. D. Stevenson, J. R. Stone, and M. R. Strayer, Phys. Rev. C **71**, 064328 (2005).
[39] A. S. Umar and V. E. Oberacker, Phys. Rev. C **71**, 034314 (2005).
[40] A. S. Umar and V. E. Oberacker, Phys. Rev. C **73**, 054607 (2006).
[41] A. S. Umar and V. E. Oberacker, Phys. Rev. C **74**, 021601(R) (2006).
[42] A. S. Umar and V. E. Oberacker, Phys. Rev. C **74**, 061601(R) (2006); **76**, 014614 (2007).
[43] J. A. Maruhn, P.-G. Reinhard, P. D. Stevenson, and M. R. Strayer, Phys. Rev. C **74**, 027601 (2006).
[44] L. Guo, J. A. Maruhn, and P.-G. Reinhard, Phys. Rev. C **76**, 014601 (2007).
[45] V. Y. Denisov and W. Nörenberg, Eur. Phys. J. A **15**, 375 (2002).
[46] A. Dobrowolski, K. Pomorski, and J. Bartel, Nucl. Phys. **A729**, 713 (2003).
[47] M. Liu, N. Wang, Z. Li, X. Wu, and E. Zhao, Nucl. Phys. **A768**, 80 (2006).
[48] J. Skalski, Phys. Rev. C **76**, 044603 (2007).
[49] A. S. Umar, M. R. Strayer, R. Y. Cusson, P.-G. Reinhard, and D. A. Bromley, Phys. Rev. C **32**, 172 (1985).
[50] D. H. E. Gross and H. Kalinowski, Phys. Lett. **B48**, 302 (1974); Phys. Rep. **45**, 175 (1978).
[51] J. Blocki *et al.*, Ann. Phys. (NY) **113**, 330 (1978).
[52] J. Randrup and W. Swiatecki, Ann. Phys. (NY) **125**, 193 (1980).
[53] J. Randrup and W. Swiatecki, Nucl. Phys. **A429**, 105 (1984).
[54] D. M. Brink and F. Stancu, Phys. Rev. C **24**, 144 (1981).
[55] W. M. Seif, Nucl. Phys. **A767**, 92 (2006).
[56] Z. Q. Feng, G. M. Jin, and F. S. Zhang, Nucl. Phys. **A802**, 91 (2008).
[57] K. Washiyama and D. Lacroix, in preparation.
[58] L. C. Vaz, J. M. Alexander, and G. R. Satchler, Phys. Rep. **69**, 373 (1981).
[59] J. Newton, R. D. Butt, M. Dasgupta, D. J. Hinde, I. I. Gontchar, C. R. Morton, and K. Hagino, Phys. Lett. **B586**, 219 (2004); Phys. Rev. C **70**, 024605 (2004).
[60] A. S. Umar and V. E. Oberacker, arXiv:0802.1479.